PPPL
PRINCETON PLASMA
PHYSICS LABORATORY

PPPL-3695

PPPL-3695

Field Line Resonances in Quiet and Disturbed Time Three-Dimensional Magnetospheres

by

C.Z. Cheng and S. Zaharia

May 2002

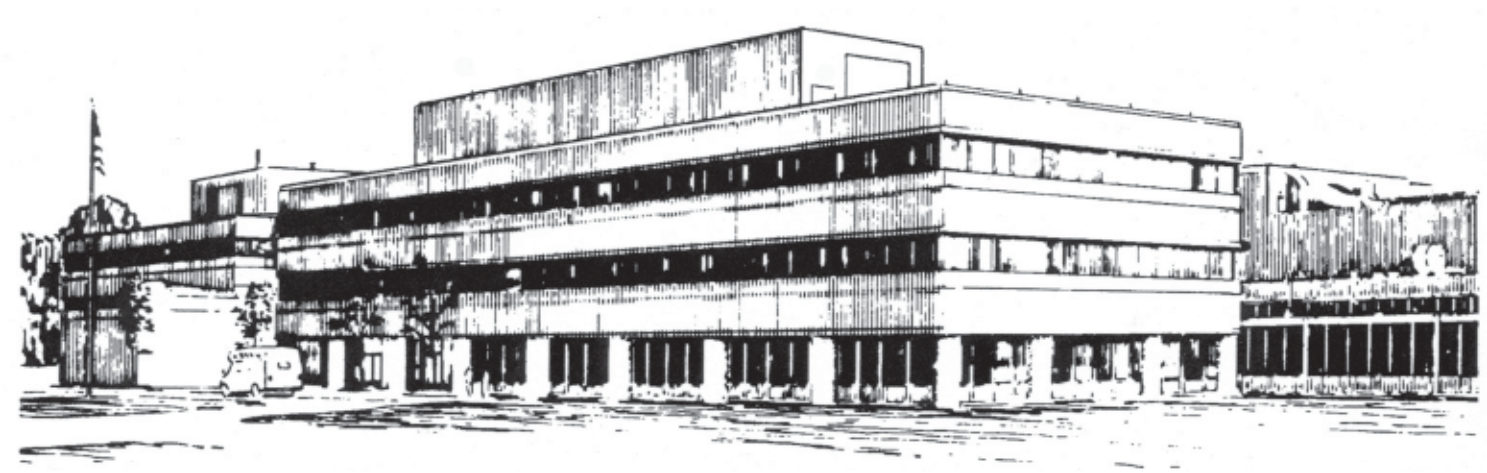

PRINCETON PLASMA PHYSICS LABORATORY
PRINCETON UNIVERSITY, PRINCETON, NEW JERSEY

Field Line Resonances in Quiet and Disturbed Time Three-Dimensional Magnetospheres

C. Z. Cheng and S. Zaharia
Princeton University, Plasma Physics Laboratory, Princeton, NJ

Received _____; accepted _____

submitted to *Journal of Geophysical Research*, 2002

Short title: FIELD LINE RESONANCE

Abstract.

Numerical solutions for field line resonances (FLR) in the magnetosphere are presented for three-dimensional equilibrium magnetic fields represented by two Euler potentials as $\mathbf{B} = \boldsymbol{\nabla}\psi \times \boldsymbol{\nabla}\alpha$, where ψ is the poloidal flux and α is a toroidal angle-like variable. The linearized ideal MHD equations for FLR harmonics of shear Alfvén waves and slow magnetosonic modes are solved for plasmas with the pressure assumed to be isotropic and constant along a field line. The coupling between the shear Alfvén waves and the slow magnetosonic waves is via the combined effects of geodesic magnetic field curvature and plasma pressure. Numerical solutions of the FLR equations are obtained for a quiet time magnetosphere as well as a disturbed time magnetosphere with a thin current sheet in the near-Earth region. The FLR frequency spectra in the equatorial plane as well as in the auroral latitude are presented. The field line length, magnetic field intensity, plasma beta, geodesic curvature and pressure gradient in the poloidal flux surface are important in determining the FLR frequencies. In general, the computed shear Alfvén FLR frequency based on the full MHD model is larger than that based on the commonly adopted cold plasma model in the $\beta_{eq} > 1$ region. For the quiet time magnetosphere the shear Alfvén resonance frequency decreases monotonically with the equatorial field line distance which reasonably explains the harmonically structured continuous spectrum of the azimuthal magnetic field oscillations as a function of L shell in the $L \leq 9\,R_E$ region. However, the FLR frequency spectrum for the disturbed time magnetosphere with a near-Earth thin current sheet is substantially different from that for the quiet time magnetosphere for $R > 6\,R_E$, mainly due to shorter field line length due to magnetic field compression by solar wind, reduced magnetic field intensity in the high β current sheet region, azimuthal pressure gradient and geodesic magnetic field curvature.

1. Introduction

Field line resonances (FLRs) with multi-harmonic frequencies have been observed extensively, for example, in the $2 \leq R/R_E \leq 9$ region by AMPTE/CCE [*Takahashi et al.*, 1990, 2002]. It was firmly established that they are the most commonly excited Pc 3-5 waves in the dayside magnetosphere from the plasmapause to the magnetopause [*Engebretson et al.*, 1986]. The distinctive structure in the azimuthal component, consisting of several frequency components, corresponds to the fundamental and higher harmonics of the local toroidal Alfvén resonances. The L-shell dependence of the frequency and the latitudinal dependence of wave amplitudes are unambiguous evidence for local shear Alfvén field line resonances. The excitation mechanism of these pulsations has also been observed to be due to external sources. Correlating the CCE magnetic field data with simultaneous solar wind data from AMPTE/IRM, *Engebretson et al.* [1987] found that both the direction of the interplanetary magnetic field and the velocity of the solar wind govern the amplitude of the harmonically structured magnetic pulsations. A comprehensive statistical study of the resonant harmonic waves [*Anderson et al.*, 1990] concluded that different source mechanisms can generate different harmonic modes at different local times. The dayside source may be related to the bow-shock-associated upstream waves, and the flank side strong fundamental waves may be driven by the Kelvin-Helmholtz instability generated waves. These toroidal Alfvén resonances can also be excited impulsively by a dayside pressure change embedded in the solar wind [*Potemra et al.*, 1989].

Field line resonance (FLR) has also been considered as a mechanism for the auroral arc formation. Several FLR characteristics are found to correlate well with those of auroral arcs [*Samson et al.*, 1992, 1996; *Lotko et al.*, 1998]. These include quasiperiodic poleward motion of auroral forms, narrow frequency band in luminosity power spectrum, arc duration of many hours, progressively lower frequency signal with increasing latitude, and a nearly 180° shift in wave electric and magnetic field. In addition, FLR can account

for the small arc thickness by mode conversion to inertial Alfvén waves [*Wei et al.*, 1994; *Trondsen et al.*, 1997; *Streltsov et al.*, 1998]. There is also recent interest in FLR from Fast Auroral SnapshoT (FAST) observations of several features associated with an auroral arc [*Lotko et al.*, 1998]. The reported frequency range for FLR in the night sector is $1 - 4$ mHz at auroral latitudes. There are varying degrees of success in matching observed frequencies with the theoretical ones. The FLR frequencies calculated for a dipole magnetosphere are generally at least one order of magnitude larger than those observed. A significant reduction of FLR frequency can be achieved by stretching the magnetic field line length either with an empirical magnetic field model [*Rankin et al.*, 2000] or a self-consistent equilibrium with stretched magnetic field [*Lui and Cheng*, 2001].

The theory of field line resonances of standing shear Alfvén waves in response to the propagation of compressional MHD waves [*Radoski*, 1966; *Cummings et al.*, 1969; *Tataronis and Grossmann*, 1973; *Chen and Hasegawa*, 1974; *Southwood*, 1974; *Cheng and Chance*, 1986; *Cheng et al.*, 1993] seemed to be able to explain the basic features of low- to mid- frequency (Pc 3-5) transverse waves. The corresponding eigenfrequencies for the transverse shear Alfvén waves standing along the field lines vary spatially and constitute the so-called shear Alfvén continuum. For an excitation frequency matching an eigenfrequency inside the shear Alfvén continuum, the wave resonance generates perturbations that are radially singular near the particular resonant magnetic field surface. However, most FLR theories have been limited to the cold plasma model in simple one-dimensional straight magnetic field configuration [*Southwood and Kivelson*, 1986], or in a dipole field geometry [*Chen and Cowley*, 1989; *Lee and Lysak*, 1990], or in stretched magnetic fields based on empirical models such as the T96 model [*Rankin et al.*, 2000]. In a realistic magnetosphere, besides being nonuniform in the radial direction, the Alfvén velocity is also nonuniform in the azimuthal direction as well as in the direction along the ambient magnetic field, the plasma pressure is finite, and the particles are trapped in the low magnetic field region. By assuming that the pressure is

only a function of the poloidal flux (or L-shell) the continuous FLR and discrete spectra of shear Alfvén waves and slow magnetosonic modes for two-dimensional axisymmetric equilibrium magnetic field models have been studied [*Cheng and Chance*, 1986; *Cheng et al.*, 1993; *Lui and Cheng*, 2001].

In general, the MHD model with isotropic pressure dictates that the plasma pressure is constant along a field line, but can vary from field line to field line. With the magnetospheric magnetic field represented by two Euler potentials as $\mathbf{B} = \boldsymbol{\nabla}\psi \times \boldsymbol{\nabla}\alpha$, where ψ is the poloidal flux and α is a toroidal angle-like variable, the plasma pressure can be written as $P = P(\psi, \alpha)$. Recently we have reformulated the ideal MHD eigenmode equations for isotropic pressure distributions $P(\psi, \alpha)$ in a form that provides a better physical representation of the MHD continuous FLR spectra in general three-dimensional magnetic field geometries [*Cheng*, 2002]. The FLR equations that represent two branches (shear Alfvén waves and slow magnetosonic waves) of the MHD continuous spectra are naturally obtained in the formulation. A new term due to the product of $\partial P/\partial\alpha$ and the geodesic magnetic field curvature is found for the shear Alfvén waves. These two branches couple through the combined effect of geodesic magnetic field curvature and plasma pressure as was obtained previously [*Cheng and Chance*, 1986; *Cheng et al.*, 1993].

In this paper we present numerical solutions of the FLR equations for three-dimensional quasi-static magnetospheric equilibrium fields. In particular, we present results for two different states of the magnetosphere: a quiet time magnetosphere as well as a disturbed time magnetosphere with a near-Earth thin current sheet. In Section 2 we present MHD FLR equations and a Lagrangian variational principle for the FLR equations. In Section 3 we present the equilibrium solutions for a quiet time magnetosphere and a disturbed time magnetosphere as well as the shear Alfvén wave and slow magnetosonic mode FLR frequency spectrum for both magnetospheric states. For the quiet time magnetosphere the shear Alfvén resonance frequency decreases

monotonically with the L shell distance and scales as $L^{-4}\rho^{-1/2}$, which reasonably explains the harmonically structured continuous spectrum of the azimuthal magnetic field oscillations observed by AMPTE/CCE [*Engebretson et al.*, 1986; *Takahashi et al.*, 1990, 2002] in the $L \leq 9\,R_E$ region. However, the FLR frequency spectrum for the disturbed time magnetosphere with a near-Earth thin current sheet is substantially different from that for the quiet time magnetosphere for $R > 6\,R_E$ mainly due to shorter field line length due to magnetic field compression by solar wind, reduced magnetic field intensity in the high β current sheet region, azimuthal pressure gradient and geodesic magnetic field curvature. Finally, in Section 4 a summary of the major results is given, and future efforts involving global computation of wave propagation are discussed.

2. MHD Field Line Resonance Equations in 3D Fields

We consider quasi-static magnetospheric equilibria described by the system of equations

$$\begin{aligned} \mathbf{J} \times \mathbf{B} &= \boldsymbol{\nabla} P, \\ \boldsymbol{\nabla} \times \mathbf{B} &= \mathbf{J}, \\ \boldsymbol{\nabla} \cdot \mathbf{B} &= 0, \end{aligned} \tag{1}$$

where $\mathbf{J}$, $\mathbf{B}$, and P are the equilibrium current density, magnetic field, and plasma pressure, respectively. The above equilibrium equations can be cast into the following form:

$$\boldsymbol{\nabla}_\perp (P + B^2/2) = \boldsymbol{\kappa} B^2, \tag{2}$$

where $\boldsymbol{\kappa} = (\mathbf{B}/B)\cdot\boldsymbol{\nabla}(\mathbf{B}/B)$ is the magnetic field curvature and the subscript $\perp$ indicates the direction perpendicular to $\mathbf{B}$. For a general three dimensional magnetospheric equilibrium with nested flux surfaces, the magnetic field can be expressed as

$$\mathbf{B} = \boldsymbol{\nabla}\psi \times \boldsymbol{\nabla}\alpha, \tag{3}$$

where ψ and α are three-dimensional functions of the configuration space variable $\mathbf{x}$. We choose ψ to be the magnetic flux function labeling the nested flux surfaces and α to be an angle-like variable. Both ψ and α are constant along magnetic field lines, and the lines where surfaces of constant ψ and surfaces of constant α intersect represent magnetic field lines. Because $\mathbf{B} \cdot \boldsymbol{\nabla} P = 0$, $P = P(\psi, \alpha)$ is constant along field lines. However, we note that the plasma density is allowed to vary along the field lines. For magnetospheric magnetic fields α is a periodic function of toroidal angle ϕ in the cylindrical (R, ϕ, z) coordinate system to ensure the periodicity constraint on each flux surface.

With the time dependence of perturbed quantities as $e^{-i\omega t}$, the linearized ideal MHD equations governing the asymptotic behavior of the perturbed quantities are the momentum equation

$$\rho\omega^2 \boldsymbol{\xi} = \boldsymbol{\nabla}\delta p + \delta\mathbf{B} \times \mathbf{J} + \mathbf{B} \times (\boldsymbol{\nabla} \times \delta\mathbf{B}), \tag{4}$$

the equation of state

$$\delta p + \boldsymbol{\xi} \cdot \boldsymbol{\nabla} P + \Gamma_s P \boldsymbol{\nabla} \cdot \boldsymbol{\xi} = 0, \tag{5}$$

the Faraday's law

$$i\omega\delta\mathbf{B} = \boldsymbol{\nabla} \times (\delta\mathbf{E}), \tag{6}$$

and the Ohm's law

$$\delta\mathbf{E} = \boldsymbol{\xi} \times \mathbf{B}, \tag{7}$$

where $\boldsymbol{\xi}$ is the usual fluid displacement vector, $\delta\mathbf{B}$ is the perturbed magnetic field, δp is the perturbed plasma pressure, ρ is the total plasma mass density, $\delta\mathbf{E}$ is the perturbed electric field, and $\Gamma_s = 5/3$ is the ratio of specific heats.

First, we decompose the displacement vector and perturbed magnetic field as

$$\boldsymbol{\xi} = \frac{\xi_\psi \boldsymbol{\nabla}\psi}{|\boldsymbol{\nabla}\psi|^2} + \frac{\xi_s(\mathbf{B} \times \boldsymbol{\nabla}\psi)}{B^2} + \frac{\xi_b \mathbf{B}}{B^2}, \tag{8}$$

and

$$\delta\mathbf{B} = \frac{Q_\psi \boldsymbol{\nabla}\psi}{|\boldsymbol{\nabla}\psi|^2} + \frac{Q_s(\mathbf{B}\times\boldsymbol{\nabla}\psi)}{|\boldsymbol{\nabla}\psi|^2} + \frac{Q_b\mathbf{B}}{B^2}, \tag{9}$$

where $\xi_\psi = \boldsymbol{\xi}\cdot\boldsymbol{\nabla}\psi$, $\xi_s = \boldsymbol{\xi}\cdot\mathbf{B}\times\boldsymbol{\nabla}\psi/|\boldsymbol{\nabla}\psi|^2$, $\xi_b = \boldsymbol{\xi}\cdot\mathbf{B}$, $Q_\psi = \delta\mathbf{B}\cdot\boldsymbol{\nabla}\psi$, $Q_s = \delta\mathbf{B}\cdot\mathbf{B}\times\boldsymbol{\nabla}\psi/B^2$, $Q_b = \delta\mathbf{B}\cdot\mathbf{B}$. We also define $\Delta = \boldsymbol{\nabla}\cdot\boldsymbol{\xi}$, and the geodesic curvature $\kappa_s = 2\boldsymbol{\kappa}\cdot\mathbf{B}\times\boldsymbol{\nabla}\psi/B^2$. A set of global MHD eigenmode equations and field line resonance equations have been derived in the paper by *Cheng* [2002]. The FLR equations are

$$\left[\mathbf{B}\cdot\boldsymbol{\nabla}\left(\frac{|\boldsymbol{\nabla}\psi|^2}{B^2}\mathbf{B}\cdot\boldsymbol{\nabla}\xi_s\right) + \frac{\rho\omega^2|\boldsymbol{\nabla}\psi|^2}{B^2}\xi_s + \kappa_s\frac{\partial P}{\partial\alpha}\xi_s\right] + \Gamma_s P\kappa_s\Delta = 0, \tag{10}$$

and

$$\left[\mathbf{B}\cdot\boldsymbol{\nabla}\left(\frac{\Gamma_s P}{\rho\omega^2 B^2}\mathbf{B}\cdot\boldsymbol{\nabla}\Delta\right) + \frac{B^2+\Gamma_s P}{B^2}\Delta\right] + \kappa_s\xi_s = 0. \tag{11}$$

Since Eqs. (10) and (11) can be combined to form a fourth order ordinary differential equation along the field line with the coefficients being all non-singular, the eigenvalues ω must be discrete for closed field lines. Thus, for each field line a discrete set of eigenvalues ω_n, where the index $n = 0, 1, 2, ...$, can be found with the corresponding eigenfunctions ξ_{sn} and Δ_n satisfying appropriate boundary conditions along closed field lines. Note that ξ_{sn} and Δ_n are linearly dependent through Eqs. (10) and (11). Because the field lines are continuous in space, each ω_n takes a continuous range of values for different field lines and forms a continuous spectrum.

A Lagrangian functional δL can be obtained from Eqs. (10) and (11) and is given by

$$\begin{aligned}\delta L = \int_{s_1}^{s_2}\frac{ds}{B}\Bigg\{&\rho\omega^2\left(\frac{|\boldsymbol{\nabla}\psi|^2}{B^2}|\xi_s|^2 + B^2|Z|^2\right)\\ &-\left[\frac{|\boldsymbol{\nabla}\psi|^2}{B^2}|\mathbf{B}\cdot\boldsymbol{\nabla}\xi_s|^2 - \kappa_s\frac{\partial P}{\partial\alpha}|\xi_s|^2 + \frac{\Gamma_s P B^2}{\Gamma_s P + B^2}|\kappa_s\xi_s + \mathbf{B}\cdot\boldsymbol{\nabla}Z|^2\right]\Bigg\} = 0\end{aligned} \tag{12}$$

where $Z = \Gamma_s P(\mathbf{B}\cdot\boldsymbol{\nabla}\Delta)/\rho\omega^2 B^2$, the boundary condition $\xi_s^*\mathbf{B}\cdot\boldsymbol{\nabla}\xi_s = \Delta Z^* = 0$ at the field line end points is assumed, and we have also made use of Eq. (11) to substitute Δ

in terms of ξ_s and $\mathbf{B} \cdot \boldsymbol{\nabla} Z$. It is straightforward to verify that Eqs. (10) and (11) are a consequence of the requirement that the functional δL is stationary.

It is clear that there are only two branches of MHD FLRs - the shear Alfvén branch (Eq. (10)) and the slow magnetosonic branch (Eq. (11)), and the coupling of these two branches is through the geodesic magnetic field curvature κ_s and plasma pressure. We also note that there is an additional term in the shear Alfvén equation due to the pressure gradient in the $\mathbf{B} \times \boldsymbol{\nabla}\psi$ direction. In the cold plasma limit ($P = 0$), the slow magnetosonic wave no longer exists. Eq. (10) then reduces to a second order ordinary differential equation for ξ_s and describes the shear Alfvén resonance (toroidal magnetic field resonance) in the cold plasma limit previously investigated by *Cummings et al.* [1969]. However, from Eq. (11) $\Delta = -\kappa_s \xi_s$ and thus the shear Alfvén waves retain a finite plasma compressibility if the geodesic magnetic field curvature κ_s is non-vanishing.

3. Continuous Field Line Resonance Spectrum in 3D Magnetospheric Fields

In the following we present numerical solutions for the field line resonance frequencies for the shear Alfvén and slow magnetosonic continuous spectrum in three-dimensional magnetospheric equilibrium fields with high β plasma. A numerical code, the MAG-3D code [*Cheng*, 1995], has been developed to solve the force balance equation in a domain bounded by the specified inner most and outer most flux surfaces with a prescribed pressure distribution in the equatorial plane. The innermost and outermost constant ψ surfaces are imposed as those obtained from the Tsyganenko's T-96 model [*Tsyganenko*, 1995; *Tsyganenko and Stern*, 1996]. In terms of the (ψ, θ, α) flux coordinate system the Jacobian is $\mathcal{J}^{-1} = \nabla\psi \times \nabla\alpha \cdot \nabla\theta$. In the MAG-3D code we choose ψ and α to be coincide with the dipole field flux ψ_d and toroidal angle ϕ respectively on the Earth's surface with the dipole field represented as $\mathbf{B}_d = \nabla\psi_d \times \nabla\phi$. We also choose the field-

aligned θ coordinate such that equal θ interval corresponds to equal arc length along a field line. Moreover, θ is normalized for all field lines such that $\theta = 0, \pi$ correspond to the end points of field lines. In the following we present the numerical solutions of the shear Alfvén and slow mode continuum spectrum in two equilibrium fields: a quiet time equilibrium and a disturbed time equilibrium with a thin current sheet in the near-Earth plasma sheet region. The numerical solutions are obtained by solving the Lagrangian equation, Eq. (12) with a finite element method. The basis functions are chosen to be $\sin(l\theta)$, where $0 \leq \theta \leq \pi$ and $l = 1, 2, ...$, such that each basis function satisfies a reflecting boundary condition, and thus the perturbations ξ_s and $\boldsymbol{\nabla} \cdot \boldsymbol{\xi}$ vanish on the Earth's surface for each field line.

3.1. Quiet Time Magnetospheric Fields

A quiet time 3D magnetospheric equilibrium field is obtained with the pressure chosen to be a function of radial distance in the equatorial plane. $P(R)$ in unit of nPa is chosen to be the empirical profile obtained by *Spence and Kivelson* [1993], $P(R) = 89e^{-0.59|R|} + 8.9|R|^{-1.53}$. The innermost and outermost constant ψ surfaces are imposed as those obtained from the Tsyganenko's T-96 model [*Tsyganenko*, 1995; *Tsyganenko and Stern*, 1996] with parameters typical of a quiet-time state: $B_{zIMF} = 10$ nT, $B_{yIMF} = 0$, $D_{st} = 0$, and the solar wind dynamic pressure $P_{sw} = 0.55$ nPa. Figure 1 shows constant equilibrium flux surfaces of a quiet equilibrium in the noon-midnight meridian plane as well as in the equatorial plane. Fig. 2 shows the equatorial values of pressure (in nPa), magnetic field B_{eq} (in nT) and the plasma beta β_{eq} along the sun-Earth axis. β_{eq} is less than unity on the day side, but on the night side becomes larger than unity for $R > 7\,R_E$, increases with R and reaches to about 60 at $23\,R_E$. Figure 3 shows the azimuthal current density (J_ϕ in unit of nA/m^2) distribution in the midnight meridian and the equatorial plane. It is clear that J_ϕ is larger on the night side than on the day side.

Figure 1.

Figure 2.

Figure 3.

3.2. Continuous Field Line Resonance Spectrum in Quiet Time Magnetospheric Fields

Once a 3D quasi-static magnetospheric equilibrium is known we can compute the FLR solutions for each field line. However, in computing the FLR frequency we need to specify the mass density along field lines. In the cold plasma model there is no constraint on the plasma density, and various density models had been employed by *Cummings et al.* [1969] for computing the shear Alfvén FLR frequency. However, in the isotropic pressure MHD model the warm plasma density is constrained to be constant along a magnetic field line to maintain force balance along a field line, and from adiabatic pressure law the mass density is proportional to $P^{-5/3}$. We also note that there is a cold plasma component which can give rise to nonuniform density along the field line. Nevertheless, because there is not enough information on the cold plasma density, we will assume for simplicity the plasma density to be constant along the field line and choose it to be a function of radius in the equatorial plane: $\rho(R) = 10\,(R_{geos}/R)^4 m_p/cm^3$, where $R_{geos} = 6.6\,R_E$ is the geosynchronous orbit distance and m_p is the proton mass. When the actual mass density distribution is known, the frequency can be recalculated easily with the actual density from the results given in this paper.

Figure 4.

First, we show the solutions of un-coupled equations for the shear Alfvén wave and slow magnetosonic wave FLRs separately, i.e., by neglecting the coupling terms, $\Gamma_s P \kappa_s \Delta$ in Eq. (10) and $\kappa_s \xi_s$ in Eq. (11). The square of frequency f (in mHz) of FLR harmonics versus the field line equatorial distance R (in R_E) for field lines with a constant α that corresponds to the local time 22:48:00 on the Earth surface are plotted in Fig. 4 for (a) the shear Alfvén FLR in the cold plasma model, (b) the un-coupled shear Alfvén FLR in the warm plasma MHD model, (c) the un-coupled slow magnetosonic mode FLR in the warm plasma MHD model, and (d) shear Alfvén waves and slow magnetosonic modes in the coupled warm plasma MHD model. The un-coupled shear Alfvén wave

FLR frequency for warm plasma is given by

$$\omega^2 = \int_{s_1}^{s_2} \frac{ds}{B} \left[\frac{|\boldsymbol{\nabla}\psi|^2}{B^2} |\mathbf{B}\cdot\boldsymbol{\nabla}\xi_s|^2 - \kappa_s \frac{\partial P}{\partial \alpha} |\xi_s|^2 \right] / \int_{s_1}^{s_2} \frac{ds}{B} \frac{\rho |\boldsymbol{\nabla}\psi|^2}{B^2} |\xi_s|^2. \tag{13}$$

The shear Alfvén FLR frequency has been commonly calculated with the cold plasma model. Figure 4(a) shows that f^2 of the shear Alfvén FLR with cold plasma model decreases as R, which is similar to the radial dependence of the Alfvén speed, $V_A = B/\rho^{1/2}$, (shown in Fig. 5(a)) divided by the field line length. By comparing Fig. 4(a) with Fig. 4(b) it is clear that the new term with coefficient $\kappa_s \partial P/\partial\alpha$ reduces f^2 in the high β_{eq} region for all harmonics. This is mainly because the new term $\kappa_s \partial P/\partial\alpha > 0$ ($\kappa_s < 0$ and $\partial P/\partial\alpha < 0$ in the pre-midnight sector and $\kappa_s > 0$ and $\partial P/\partial\alpha > 0$ in the post-midnight sector). From Fig. 4(b) the effect on the shear Alfvén fundamental (n = 0) harmonic is more pronounced due to low frequency values and f^2 becomes negative (unstable) for $R > 15.5\, R_E$.

Figure 5.

The un-coupled slow magnetosonic mode FLR frequency is given by

$$\omega^2 = \int_{s_1}^{s_2} \frac{ds}{B} \frac{\Gamma_s P}{\rho B^2} |\mathbf{B}\cdot\boldsymbol{\nabla}\Delta|^2 / \int_{s_1}^{s_2} \frac{ds}{B} \frac{B^2 + \Gamma_s P}{B^2} |\Delta|^2. \tag{14}$$

For $\Gamma_s P \gg B^2$ the slow magnetosonic mode frequency approaches the shear Alfvén frequency in the cold plasma limit and is roughly given by $\omega^2 = k_\parallel^2 B^2/\rho$ in the field line average sense. For $\Gamma_s P \ll B^2$ the slow magnetosonic mode frequency is roughly given by $\omega^2 = k_\parallel^2 \Gamma_s P/\rho$ in the field line average sense. As shown in Fig. 4(c) the fundamental harmonic (n = 0) frequency is very small ($\ll 1$ mHz) even in the region where $\beta_{eq} \gg 1$. This is mainly because the fundamental harmonic (n = 0) mode structure is extended along the field line and $\Gamma_s P$ is much smaller than B^2 except in the lower latitude region of the field lines. However, for the second (n = 1) and higher harmonics the slow magnetosonic mode structure is more localized in the lower latitude region and their frequencies are larger with $f > 3$ mHz as shown in Fig. 4(c). We also note that the slow mode frequency decreases as R (or equatorial beta value β_{eq}) increases, except for the n = 1, 2 harmonics whose frequencies become flat for $R > 12\, R_E$.

Fig. 4(d) shows f^2 vs. R for the harmonic solutions of the coupled equations. Including the coupling between the shear Alfvén and slow magnetosonic modes, the fundamental harmonic (n = 0) of shear Alfvén modes is stabilized ($f^2 > 0$), but for other harmonics their frequencies are much less affected and are slightly higher in the high β_{eq} region. Clearly, the coupling causes f^2 of the fundamental harmonic shear Alfvén mode to increase in the $\beta_{eq} > 1$ region ($R > 10\,R_E$). For slow magnetosonic modes the frequencies of all harmonics are smaller than those of shear Alfvén waves with similar nodal structures along **B**. The slow mode frequencies are also weakly affected by the coupling except when the frequency of shear Alfvén modes crosses that of the slow modes; the coupling of these two modes causes a small frequency gap to form in the continuous spectrum. Note that the fundamental harmonic (n = 0) shear Alfvén modes have higher (lower) frequency than the second harmonic (n = 1) slow modes for $R > 8\,R_E$ ($R < 8\,R_E$). The harmonically structured continuous spectrum of the azimuthal magnetic field oscillations as a function of R observed by AMPTE/CCE for $R \leq 8.8\,R_E$ [*Engebretson et al.*, 1986] can be reasonably interpreted by the shear Alfvén resonance frequency which scales as $R^{-4}\rho^{-1/2}$ [*Anderson et al.*, 1990; *Takahashi et al.*, 1990, 2002]. However, no observational evidence has been established for the slow magnetosonic continuous spectrum in the magnetosphere. This may be because the slow magnetosonic waves are easily Landau damped if ion temperature is roughly equal or larger than electron temperature as is usually the case in the magnetosphere.

Figure 6.

Figure 7.

Figs. 6 and 7 show the contours of fundamental harmonic (n = 0) shear Alfvén FLR frequency (in mHz) in the equatorial plane and in the northern polar ionosphere, respectively. The constant FLR frequency contours in the near Earth (lower latitude) region form closed surfaces that are slightly different from the constant flux surfaces in the night side. However, the constant FLR frequency surfaces in the higher latitude region deviate substantially from the constant flux surfaces. In particular, in the night side high latitude region (the tail region) the constant FLR frequency surfaces form

closed contours localized around midnight. It is to be noted that a different equatorial density profile will yield a different global behavior of the FLR frequency. The behavior of the FLR frequencies can be understood from Fig.8 which shows the contours of Alfvén speed, $V_A = B/\rho^{1/2}$, and slow magnetosonic speed, $C_s = (\Gamma_s P B^2/\rho(\Gamma_s P + B^2))^{1/2}$, in the equatorial plane. Note that the Alfvén speed is similar to that presented by *Moore et al.* [1987] for $6 < R/R_E < 12$ on the night side. It is clear that shear Alfvén (slow magnetosonic) FLR frequency behaves qualitatively similar to the shear Alfvén (slow magnetosonic) speed divided by the field line length. It is to be reiterated that the R^{-4} dependence of mass density distribution is idealized and an empirical mass density distribution can be used to adjust the results presented here.

Figure 8.

3.3. A Disturbed Time Magnetospheric Equilibrium Field with Thin Current Sheet

The disturbed-state equilibrium with thin current sheet was obtained by specifying the innermost and outermost flux surfaces obtained from the T96 model with parameters typical of disturbed times, i.e. southward IMF, negative DST and increased solar wind dynamic pressure. The particular values chosen are: $B_{zIMF} = -2$ nT, $B_{yIMF} = 0$, $D_{st} = -40$ nT and $P_{sw} = 3$ nPa. The pressure profile was modified from the one used in the quiet-time case to reflect the typical pressure changes observed during active magnetospheric conditions [e.g., *Lui et al.*, 1987]. We still assume $P = P(R)$ in the equatorial plane, but as seen in Fig. 9 which shows the pressure (in nPa), magnetic field (in nT) and the plasma beta along the sun-Earth axis, we have chosen significantly larger pressure value from $3.5\,R_E$ to $9\,R_E$, than the empirical quiet time value obtained by *Spence and Kivelson* [1993] in order to model the observed pressure. Figure 10 shows constant equilibrium flux surfaces of a disturbed time equilibrium in the noon-midnight meridian plane and in the equatorial plane. It is to be noted that the outer boundary flux surface provided by the T-96 model is strongly compressed in the north-south direction by

the solar wind and thus the field line length is shorter in comparison with the quiet time magnetosphere for the same equatorial crossing point. Figure 11 shows the azimuthal current density (J_ϕ) distribution in (a) the midnight meridian plane and (b) the equatorial plane. It is clear that a thin current sheet is located in the near-Earth region from $x \simeq -6$ to $-9\,R_E$, from $z \simeq -0.5$ to $0.5\,R_E$ and from $y \simeq -3$ to $3\,R_E$. In the thin current sheet region a shallow magnetic well is dug at around $x = -7.5\,R_E$, and the plasma β_{eq} is enhanced to over 10 in the radial region from $x = -6$ to $-9\,R_E$ (peaks at about 32 at about $x = -7\,R_E$) which is much larger than the quiet time value of $0.5 \leq \beta_{eq} \leq 1.5$ in the same radial region (see Fig. 2).

Figure 9.

Figure 10.

Figure 11.

Figure 12.

3.4. Continuous Field Line Resonance Spectrum in a Disturbed Time Magnetospheric Field with Thin Current Sheet

We choose the density profile to be the same as for the quiet time magnetosphere to eliminate the effect of density on the FLR frequency when comparing these two different states of the magnetosphere. The mass density profile is chosen as a function of radius in the equatorial plane: $\rho(R) = 10\,(R_{geos}/R)^4 m_p/cm^3$, where $R_{geos} = 6.6\,R_E$ is the geosynchronous orbit distance and m_p is the proton mass. It is interesting to note that the FLR frequency spectrum for the disturbed time case is substantially different from that of the quiet time case. Fig. 12 shows the square of frequency (in mHz) of FLR harmonics, f^2, versus the field line equatorial distance R (in R_E) for field lines with a constant α that corresponds to the local time 22:55:12 at the Earth for (a) the shear Alfvén wave FLR in the cold plasma model, (b) the un-coupled shear Alfvén wave FLR in the warm plasma MHD model, (c) the un-coupled slow mode FLR in the warm plasma MHD model, and (d) shear Alfvén waves and slow modes in the coupled warm plasma MHD model. First, in comparing the shear Alfvén FLR frequencies for the cold plasma model for the disturbed magnetosphere shown in Fig. 12(a) and for the quiet magnetosphere shown in Fig. 4(a), they differ in two aspects: (1) the disturbed time shear Alfvén FLR frequency

in the high β_{eq} ($R > 8\,R_E$) region is higher than the quiet time value by more than 80% at $R = 15\,R_E$ and by about 30% at $R = 9\,R_E$, and (2) the frequency decreases at small R to form local minima at around $R \simeq 7\,R_E$ and then increases as R increases further. (1) is mainly because the field line length from the same equatorial distance is shorter in the disturbed magnetosphere than in the quiet time magnetosphere as shown in Figs 10 and 1. The frequency local minima are in the current sheet region and are due to the reduction of magnetic field and thus of the Alfvén speed in the magnetic well as shown in Fig. 13 (a) which shows the Alfvén speed, $V_A = B/\rho^{1/2}$, versus the field line equatorial distance R (in R_E). **Figure 13.**

The effect of the new $\kappa_s \partial P/\partial\alpha$ term on the un-coupled shear Alfvén FLR frequency can be seen by comparing Fig. 12(a) with Fig. 12(b). It is clear that the new term reduces f^2 in the high β_{eq} ($\beta_{eq} > 10$ for $R > 6\,R_E$) region for all harmonics. The effect on the fundamental (n = 0) harmonic is more pronounced due to low frequency values and f^2 becomes negative for $R > 7\,R_E$ where $\beta_{eq} \geq 10$.

The un-coupled slow magnetosonic mode FLR frequency is shown in Fig. 12(c), and the fundamental harmonic (n = 0) frequency is very small ($\ll$ 1 mHz), similar to the quiet time case because the fundamental harmonic mode structure is extended along the field line and $\Gamma_s P$ is much smaller than B^2 except in the lower latitude region of the field lines. For higher harmonics ($n \geq 1$) the slow magnetosonic mode structure is more localized in the lower latitude region and their frequencies are larger than 5 mHz which is larger than in the quiet time case as shown in Fig. 4(c). We also note that the higher harmonic ($n \geq 1$) slow mode FLR frequency increases with R at small R, peaks at around $7\,R_E$ near the current sheet region, but decreases as R further increases. The frequency peaking in the current sheet region is mainly due to shorter field line distance as R decreases and to the magnetosonic speed C_s profile variation along the field line as well as in the radial direction as shown in Fig.13(b). Note that the C_s profile has a dip in the three-dimensional current sheet region (at around $R = 7\,R_E$) due to the reduction

of magnetic field, and C_s increases rapidly away from the equatorial plane along the field line. The dip can be seen in the frequency of higher harmonics ($n > 2$) slow mode. We also note that the slow mode FLR frequency profile differs from that of the quiet time case (Fig. 4(c)) mainly because of shorter field line length and larger C_s due to larger pressure value. From Fig.13(b) the equatorial C_s is larger than the quiet time value for $R < 6\,R_E$ and $R > 12\,R_E$.

Fig. 12(d) shows f^2 vs. R for the FLR harmonic solutions of the coupled equations. Including the coupling between the shear Alfvén and slow magnetosonic modes, the fundamental harmonic (n = 0) of shear Alfvén modes is stabilized ($f^2 > 0$), but for other harmonics their frequencies are much less affected and are slightly higher in the high β_{eq} region. Clearly, the coupling causes f^2 of the fundamental harmonic shear Alfvén mode to increase in the $\beta_{eq} > 1$ region ($R > 5.5\,R_E$). It is also noted that the fundamental harmonic (n = 0) shear Alfvén mode has higher frequency than that based on the cold plasma model (shown in Fig. 12(a)) for $R > 6R_E$. For slow magnetosonic modes the frequencies of all harmonics are smaller than those of shear Alfvén waves with similar nodal structures along **B**. The slow mode frequencies are weakly increased by the coupling effect, and the increase is larger for higher harmonics because these modes experience stronger coupling in the low latitude, higher β region along a field line. Also, when the shear Alfvén mode frequency crosses the slow mode frequency, coupling of these two modes causes a small frequency gap to form in the continuous spectrum. Note that the fundamental harmonic (n = 0) shear Alfvén modes have lower frequency than the second harmonic (n = 1) slow mode in the region $13\,R_E > R > 5.5\,R_E$.

Figure 14.

Figure 15.

Figs. 14 and 15 show the contours of fundamental harmonic (n = 0) shear Alfvén FLR frequency (in mHz) in the equatorial plane and in the northern polar ionosphere, respectively. The constant FLR contours in the lower latitude region form closed surfaces that are slightly different from the constant flux surfaces in the night side. However, the constant FLR frequency surfaces in the higher latitude region deviate greatly from the

constant flux surfaces. In particular, in the night side high latitude region (the tail region) the constant FLR surfaces form closed contours localized around midnight. Moreover, for certain excitation frequencies there is more than one resonance surface. However, it is to be noted that a different equatorial density profile will yield a different global behavior of the FLR frequency.

To help understand the behavior of the FLR frequencies the contours of Alfvén speed, $V_A = B/\rho^{1/2}$, and slow magnetosonic speed, $C_s = (\Gamma_s P B^2/\rho(\Gamma_s P + B^2))^{1/2}$, in the equatorial plane are shown in Fig.16. Note that the Alfvén speed is substantially different from that presented by *Moore et al.* [1987] due to the near-Earth current sheet for $6\,R_E < R < 12\,R_E$ on the night side. It is clear that the shear Alfvén (slow magnetosonic) FLR frequencies behave qualitatively similar to the shear Alfvén (slow magnetosonic) speed divided by the field line length. It is to be reiterated that the R^{-4} dependence of mass density distribution employed here is idealized and an empirical mass density distribution can be used to adjust the results. **Figure 16.**

4. Summary and Discussions

In this paper we have presented numerical solutions of FLR resonances based on the ideal MHD model that shows two branches of FLRs, the shear Alfvén waves and slow magnetosonic modes. The calculations were performed for a quiet time magnetosphere and a disturbed time magnetosphere with a thin current sheet in the near-Earth region $(7 - 9\,R_E)$. The magnetic field is represented as $\mathbf{B} = \boldsymbol{\nabla}\psi \times \boldsymbol{\nabla}\alpha$ and a pressure distribution $P = P(\psi, \alpha)$ is assumed. The magnetospheric equilibrium magnetic fields are calculated with the MAG-3D code [*Cheng*, 1995] by specifying the outermost and inner most boundary surfaces which are obtained from the Tsyganenko's T-96 model [*Tsyganenko*, 1995; *Tsyganenko and Stern*, 1996].

As derived in our paper [*Cheng*, 2002], there is a new term in the shear Alfvén FLR equation due to the azimuthal pressure gradient, $\partial P/\partial\alpha$, which is discussed for the first

time in the literature. These two branches of FLR continuous spectra are represented by the eigenfunctions ξ_s and $\boldsymbol{\nabla} \cdot \boldsymbol{\xi}$ with corresponding eigenfrequencies ω, and they couple through the geodesic magnetic field curvature and plasma pressure. In general, the computed shear Alfvén FLR frequency in the full MHD model is larger than that based on the commonly adopted cold plasma model in the $\beta_{eq} > 1$ region. Slow magnetosonic wave frequencies are smaller than those of shear Alfvén waves with similar nodal structures along $\mathbf{B}$ even for equatorial beta value much larger than unity. For the quiet time magnetosphere the shear Alfvén resonance frequency decreases monotonically with the equatorial field line distance (or L-shell) and scales as $L^{-4}\rho^{-1/2}$, which explains reasonably well the harmonically structured continuous spectrum of the azimuthal magnetic field oscillations as a function of L-shell observed by AMPTE/CCE [*Engebretson et al.*, 1986; *Takahashi et al.*, 1990, 2002] in the $L \leq 9\,R_E$ region. However, no observational evidence has been established for the slow magnetosonic continuous spectrum in the magnetosphere. This may be because the slow magnetosonic waves are easily Landau damped if ion temperature is roughly equal or larger than electron temperature as is usually the case in the magnetosphere.

We have also found that the FLR frequency spectrum for the disturbed time magnetosphere with a near-Earth thin current sheet is substantially different from that for the quiet time magnetosphere. In particular, the shear Alfvén FLR frequencies for the disturbed magnetosphere are about 50% larger than those for the quiet time magnetosphere in the night side for $R > 6\,R_E$ mainly due to shorter field line length due to magnetic field compression by solar wind, reduced magnetic field in the high β current sheet region, pressure gradient in $\mathbf{B} \times \boldsymbol{\nabla}\psi$ direction and geodesic magnetic field curvature. Moreover, the shear Alfvén FLR frequency has a minimum in the near-Earth current sheet region. However, the slow modes FLR frequency peaks in the the near-Earth current sheet region.

Global magnetospheric ULF pulsations with frequencies in the Pc 5 range (f =

1.7 - 6.7 mHz) and below have been observed for decades in space and on the Earth [*Herron*, 1967; *Samson et al.*, 1991; *Nikutowski et al.*, 1995; *Rinnert*, 1996; *Kepko et al.*, 2002]. Observation of discrete frequencies with f = 1.3, 1.9, 2.6, 3.4, and 4.2 mHz [*Samson et al.*, 1991] have been attributed to global wave-guide modes [*Samson et al.*, 1992]. Recently, these global magnetospheric ULF pulsations are explained as driven directly from the fluctuations in the solar wind because of the good correlation between the fluctuation spectrum observed by WIND spacecraft in the upstream solar wind region and the measured spectrum by the geosynchronous satellite GOES 10 [*Kepko et al.*, 2002]. In order to study these global modes, numerical solutions of global MHD eigenmode equations must be pursued. However, if the frequencies of these global modes are inside the FLR continuous spectrum, the compressional MHD waves will be absorbed at the FLR locations and cannot propagate to the lower L-shell region. Thus, in order for the global modes to propagate to the lower L-shell region, their frequencies must be lower than the FLR frequencies. To have a better theoretical understanding of this issue, we need to solve the global MHD equations to obtain the global wave propagation property. By imposing a source disturbance at the magnetopause boundary as a boundary condition, one can obtain the L-shell dependence of the FLR power spectrum. Thus, a global MHD solution will not only provide the information of radial wave structures, but will also improve our understanding of the azimuthal variation of the FLRs.

Acknowledgments. This work is supported by the NASA grant No. W-19512 and the NSF grant No. ATM-9906142.

References

Anderson, B. J., M. J. Engebretson, S. P. Rounds, L. J. Zanetti, and T. A. Potemra, A statistical study of pc 3-5 pulsations observed by the AMPTE/CCE spacecraft magnetic filed experiment, 1, Occurrence distributions, *J. Geophys. Res.*, *95*, 10495, 1990.

Chen, L., and S. C. Cowley, On field line resonances of hydromagnetic Alfvén waves in dipole magnetic field, *Geophys. Res. Lett.*, *16*, 895–897, 1989.

Chen, L., and A. Hasegawa, A theory of long-period magnetic pulsations, 1, steady state excitation of field line resonance, *J. Geophys. Res.*, *79*, 1024–1032, 1974.

Cheng, C. Z., Three-dimensional magnetospheric equilibrium with isotropic pressure, *Geophys. Res. Lett.*, *22*, 2401, 1995.

Cheng, C. Z., MHD field line resonances and global modes in three-dimensional magnetic fields, submitted to J. Geophys. Res., 2002.

Cheng, C. Z., and M. S. Chance, Low-n shear Alfvén spectra in axisymmetric toroidal plasmas, *Phys. Fluids*, *29*, 3695–3701, 1986.

Cheng, C. Z., T. C. Chang, C. A. Lin, and W. H. Tsai, Magnetohydrodynamic theory of field line resonances in the magnetosphere, *J. Geophys. Res.*, *98*, 11,339–11,347, 1993.

Cummings, W. D., R. J. O'Sullivan, and J. P. J. Coleman, Standing Alfvén waves in the magnetosphere, *J. Geophys. Res.*, *74*, 778, 1969.

Engebretson, M. J., L. J. Zanetti, T. A. Potemra, and M. H. Acuna, Harmonically structured ULF pulsations observed by the AMPTE CCE magnetic field experiment, *Geophys. Res. Lett.*, *13*, 905, 1986.

Engebretson, M. J., L. J. Zanetti, T. A. Potemra, W. Baumjohann, and H. Luhr, Simultaneous observations of Pc 3-4 pulsations in the solar wind and in the Earth's magnetosphere, *J. Geophys. Res.*, *92*, 10053, 1987.

Herron, T. J., An average geomagnetic power spectrum for the period from 4.5 to 12,900 seconds, *J. Geophys. Res.*, *72*, 759, 1967.

Kepko, L., H. E. Spence, and H. J. Singer, ULF waves in the solar wind as direct drivers of magnetospheric pulsations, *Geophys. Res. Lett.*, accepted for publication, 2002.

Lee, D. H., and R. L. Lysak, Effects of azimuthal asymmetry on ulf waves in the dipole magnetosphere, *Geophys. Res. Lett.*, *17*, 53, 1990.

Lotko, W., A. V. Streltsov, and C. W. Carlson, Discrete auroral arc, electrostatic shock, and suprathermal electrons powered by dispersive, anomalously resistive field line resonance, *Geophys. Res. Lett.*, *25*, 4449, 1998.

Lui, A. T. Y., and C. Z. Cheng, Resonant frequency of stretched magnetic field lines based on a self-consistent equilibrium magnetosphere model, *J. Geophys. Res.*, *106*, 25793 – 25802, 2001.

Lui, A. T. Y., R. W. McEntire, and S. M. Krimigis, Evolution of the ring current during two geomagnetic storms, *J. Geophys. Res.*, *92*, 7459, 1987.

Moore, T. E., D. L. Gallagher, J. L. Horwitz, and R. H. Comfort, MHD wave breaking in the outer plasmasphere, *Geophys. Res. Lett.*, *14*, 1007, 1987.

Nikutowski, B., J. Bchner, S. Klimov, S. Romanov, A. Petrukovich, and S. Savin, Long periods of ULF wave activity in the earth's magnetotail lobes, *Adv. Space Res.*, *18*, 55, 1995.

Potemra, T. A., H. Luhr, L. J. Zanetti, K. Takahashi, R. E. Erlandson, G. T. Marklund, L. P. Block, L. G. Bloomberg, and R. P. Lepping, Multi-satellite and ground-based observations of transient ulf waves, *IEEE Trans. Geosci. Remote Sen.*, *94*, 2543, 1989.

Radoski, H. R., Magnetic toroidal resonances and vibrating field lines, *J. Geophys. Res.*, *71*, 1891, 1966.

Rankin, R., P. Frycz, and V. T. Tikhonchuk, Shear Alfvén waves on stretched field lines near midnight in the Earth's magnetosphere, *Geophys. Res. Lett.*, *27*, 3265, 2000.

Rinnert, K., Quasi-periodic precipitation with periods between 40 and 60 minutes, *Ann. Geophys.*, *14*, 707, 1996.

Samson, J. C., T. J. Hughes, F. Creutzberg, D. D. Wallis, R. A. Greenwald, and J. M.

Ruohoniemi, Observations of detached, discrete arc in association with field line resonances, *J. Geophys. Res.*, *96*, 15683, 1991.

Samson, J. C., L. R. Lyons, P. T. Newell, F. Creutzberg, and B. Xu, Proton aurora and substorm intensifications, *Geophys. Res. Lett.*, *19*, 2167, 1992.

Samson, J. C., L. L. Cogger, and Q. Pao, Observations of field line resonances, auroral arcs, and auroral vortex structures, *J. Geophys. Res.*, *101*, 17373, 1996.

Southwood, D. J., Some features of field line resonances in the magnetosphere, *Planet. Space Sci.*, *22*, 483, 1974.

Southwood, D. J., and M. G. Kivelson, The effect of parallel inhomogeneity on magnetospheric wave coupling, *J. Geophys. Res.*, *91*, 6871, 1986.

Spence, H. E., and M. G. Kivelson, Contributions of the low-latitude boundary layer to the finite width magnetotail convection model, *J. Geophys. Res.*, *98*, 15487, 1993.

Streltsov, A. V., W. Lotko, J. R. Johnson, and C. Z. Cheng, Small-scale, dispersive field line resonances in the hot magnetospheric plasma, *J. Geophys. Res.*, *103*, 26559–26572, 1998.

Takahashi, K., B. J. Anderson, and R. J. Strangeway, AMPTE/CCE observations of Pc 3-4 pulsations at L = 2 - 6, *J. Geophys. Res.*, *95*, 17,179, 1990.

Takahashi, K., R. E. Denton, and D. Gallagher, Toroidal wave frequency at L = 6 - 10: AMPTE/CCE observation and comparison with theoretical model, *J. Geophys. Res.*, accepted for publication, 2002.

Tataronis, J., and W. Grossmann, Decay of MHD waves by phase mixing, I, The sheet pinch in plane geometry, *Z. Phys.*, *261*, 203, 1973.

Trondsen, T. S., L. L. Cogger, and J. C. Samson, Asymmetric multiple auroral arcs and inertial Alfvén waves, *Geophys. Res. Lett.*, *24*, 2945, 1997.

Tsyganenko, N. A., Modeling the Earth's magnetospheric magnetic field confined within a realistic magnetopause, *J. Geophys. Res.*, *100*, 5599, 1995.

Tsyganenko, N. A., and D. P. Stern, Modeling the global magnetic field of the large-scale Birkeland current systems, *J. Geophys. Res.*, *101*, 27187, 1996.

Wei, C. Q., J. C. Samson, R. Rankin, and P. Frycz, Electron inertial effects on geomagnetic field line resonances, *J. Geophys. Res.*, *99*, 11,265, 1994.

This manuscript was prepared with the AGU LaTeX macros v3.0.

With the extension package 'AGU^{++}', version 1.2 from 1995/01/12

Figure Captions

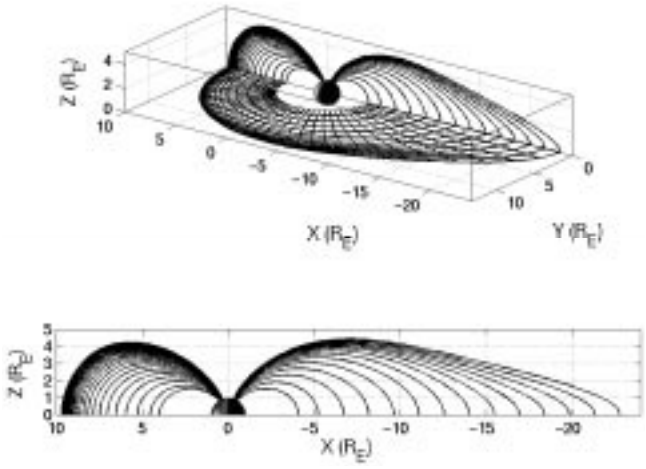

Figure 1. Constant ψ surfaces of the three-dimensional quiet time magnetospheric equilibrium in the noon-midnight meridian plane and the equatorial plane. Constant α lines are also shown in the equatorial plane. The parameters for the T-96 model are $B_{zIMF} = 10$ nT, $B_{yIMF} = 0$, $D_{st} = 0$, and the solar wind dynamic pressure $P_{sw} = 0.55$ nPa. The equatorial pressure profile is chosen as the empirical profile obtained by *Spence and Kivelson* [1993] as shown in Fig. 2.

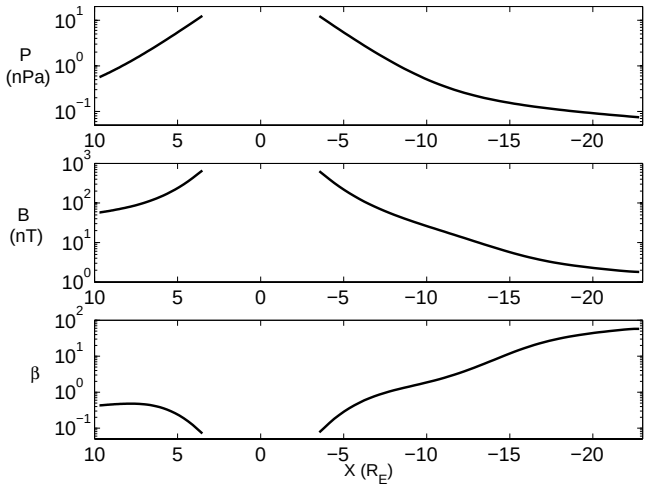

Figure 2. The plasma pressure (in nPa), magnetic field (in nT) and plasma beta along the sun-Earth axis for a quiet time magnetospheric equilibrium.

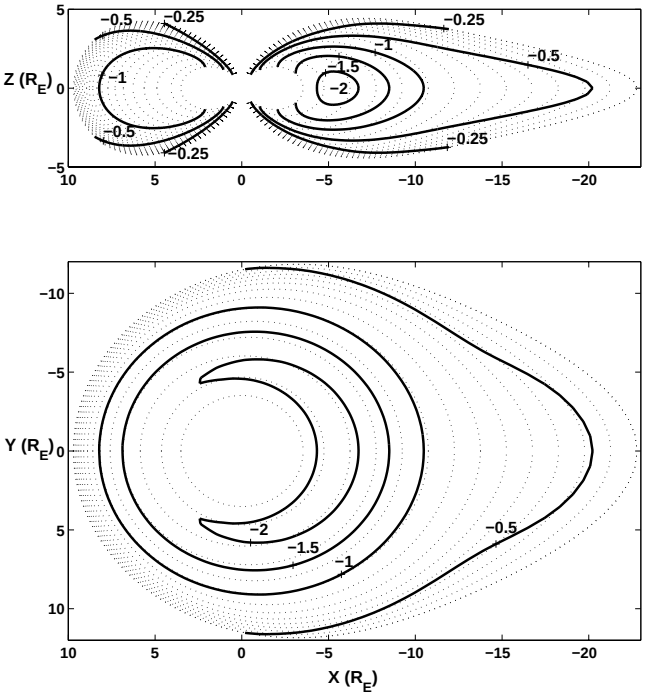

Figure 3. Contours of azimuthal current density (in nA/m^2) in the equatorial plane for a three-dimensional quiet time magnetospheric equilibrium. The azimuthal current density is larger on the nightside than on the day side. The dotted curves correspond to constant ψ values.

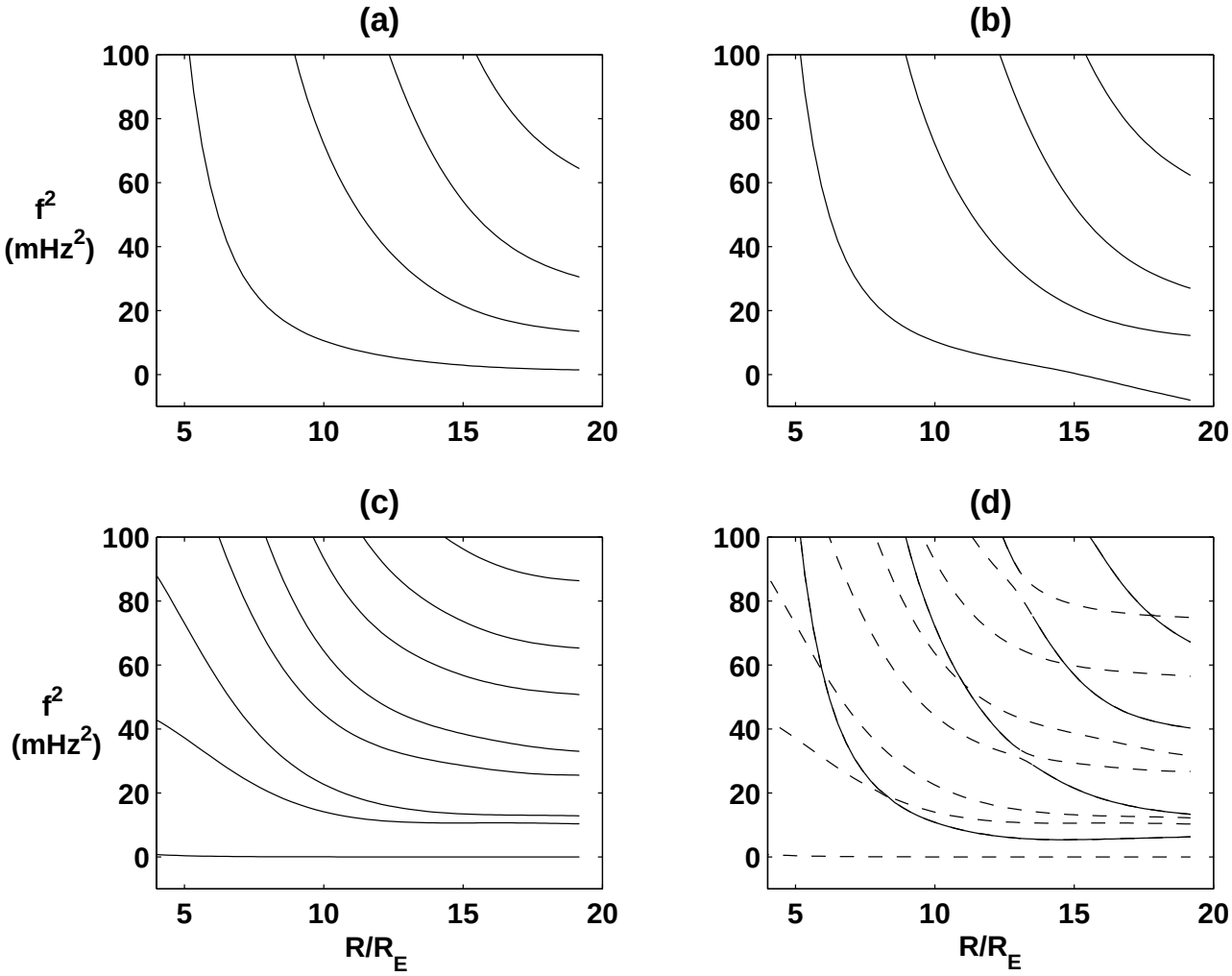

Figure 4. The square of frequency f (in mHz) of field line resonance harmonics versus the field line equatorial distance R (in R_E) is shown for field lines with a constant α that corresponds to the local time 22:48:00 at the Earth for a quiet magnetosphere. (a) is for shear Alfvén waves in the cold plasma model limit, (b) is for shear Alfvén waves in the un-coupled warm plasma MHD model, (c) is for slow magnetosonic modes in the un-coupled warm plasma MHD model, and (d) is for shear Alfvén waves (solid curves) and slow modes (dashed curves) in the coupled warm plasma MHD model.

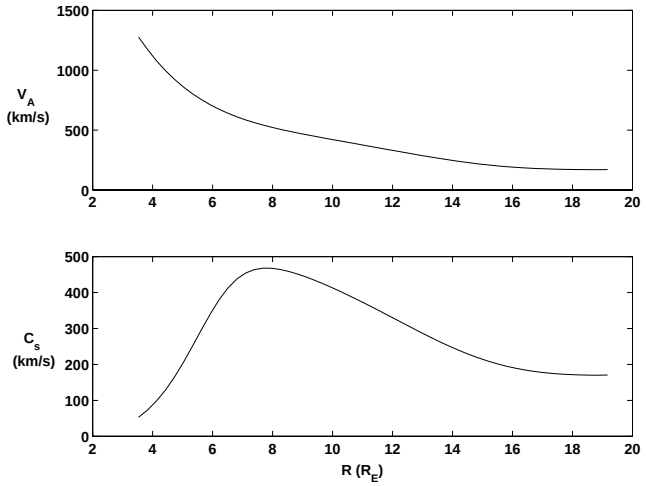

Figure 5. (a) Alfvén speed, $V_A = B/\rho^{1/2}$, and (b) slow magnetosonic speed, $C_s = (\Gamma_s P B^2/\rho(\Gamma_s P + B^2))^{1/2}$, (in km/s) versus the field line equatorial distance R (in R_E) for field lines with a constant α that corresponds to the local time 22:48:00 at the Earth for a quiet time magnetospheric equilibrium.

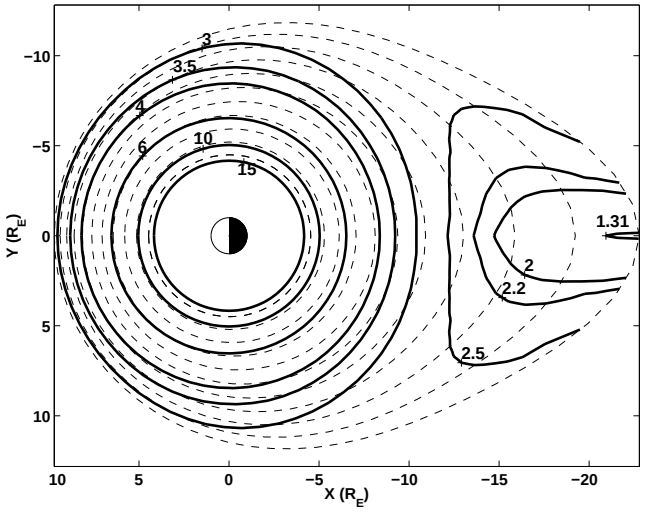

Figure 6. Contours of the fundamental harmonic shear Alfvén resonance frequency (in mHz) are plotted in the equatorial plane for a quiet time magnetosphere. The dashed curves are the intersection of constant ψ surfaces with the equatorial plane.

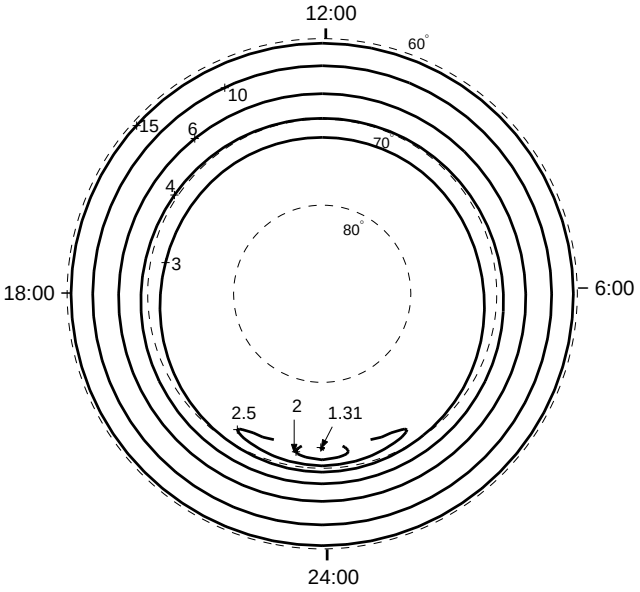

Figure 7. Contours of the fundamental harmonic shear Alfvén resonance frequency (in mHz) are plotted in the northern polar ionosphere for a quiet time magnetospheric equilibrium. The dashed circles are constant magnetic latitude lines.

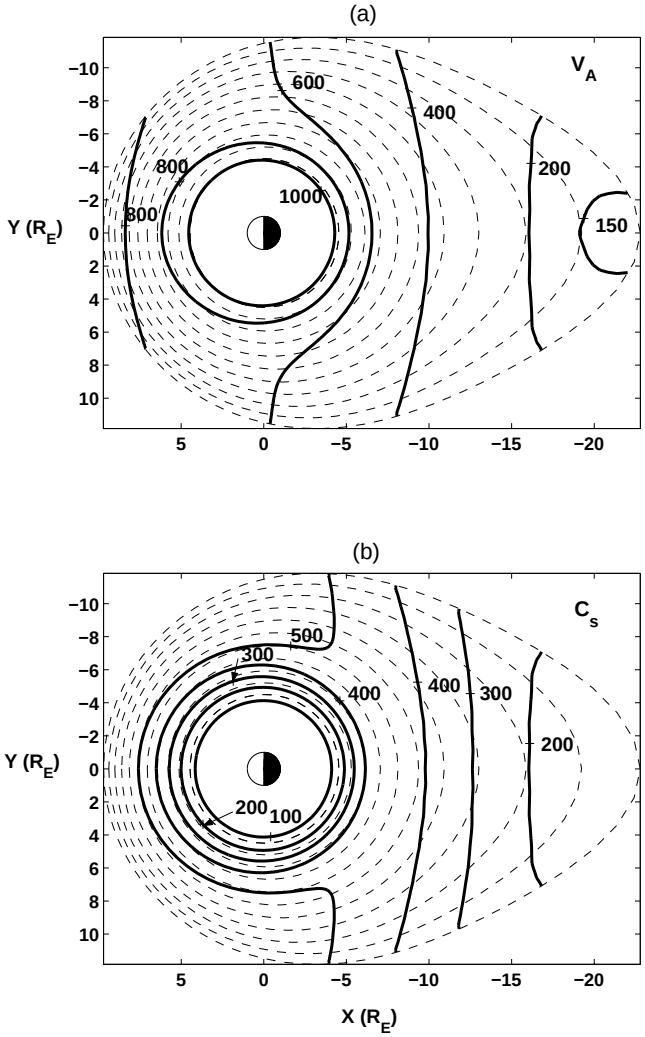

Figure 8. Contours of (a) Alfvén speed, $V_A = B/\rho^{1/2}$, and (b) slow magnetosonic speed, $C_s = (\Gamma_s P B^2/\rho(\Gamma_s P + B^2))^{1/2}$, (in km/s) in the equatorial plane for a quiet time magnetospheric equilibrium. The dashed curves are the intersection of constant ψ surfaces with the equatorial plane. ψ surfaces.

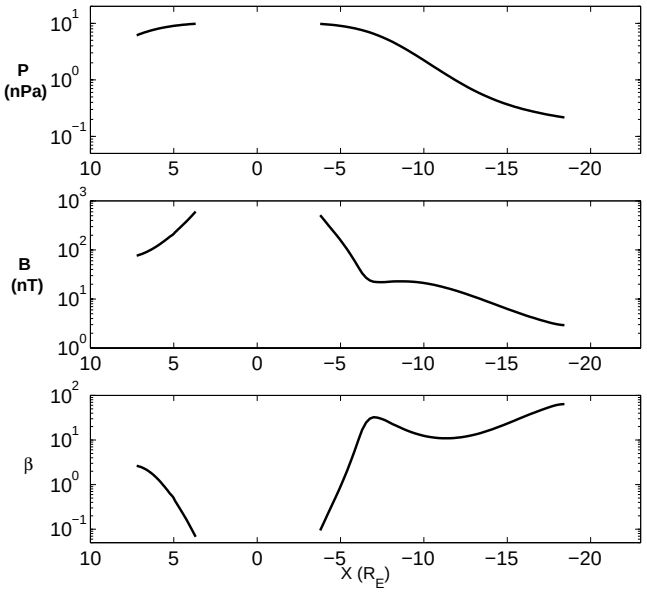

Figure 9. The plasma pressure (in nPa), magnetic field (in nT) and plasma beta along the sun-Earth axis for a disturbed time magnetosphere with a thin current sheet.

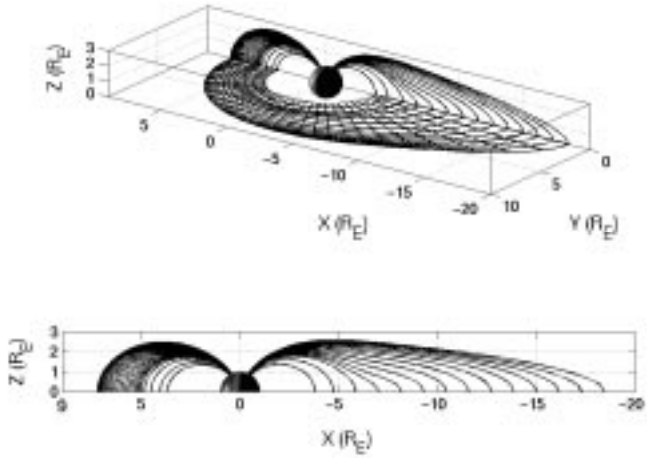

Figure 10. Constant ψ surfaces in the noon-midnight meridian plane and the equatorial plane for a three-dimensional disturbed time magnetospheric equilibrium with a thin current sheet. Constant α lines are also shown in the equatorial plane. The parameters for the T-96 model are $B_{zIMF} = -2$ nT, $B_{yIMF} = 0$, $D_{st} = -40$ nT and $P_{sw} = 3$ nPa. The equatorial pressure profile is shown in Fig. 9.

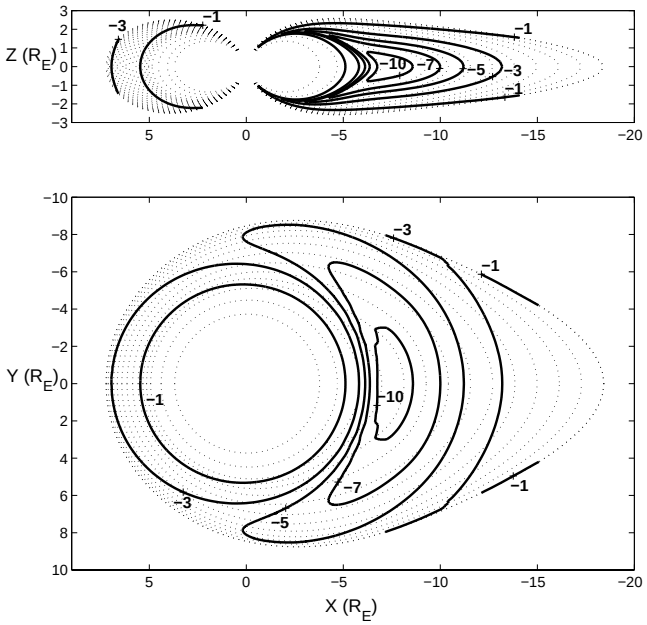

Figure 11. Contours of azimuthal current density (in nA/m^2) in the equatorial plane for a three-dimensional disturbed time magnetospheric equilibrium with a thin current sheet. The dotted curves correspond to constant ψ values. An enhanced cross tail current is formed in the current sheet region from $x = -6$ to $-9\,R_E$.

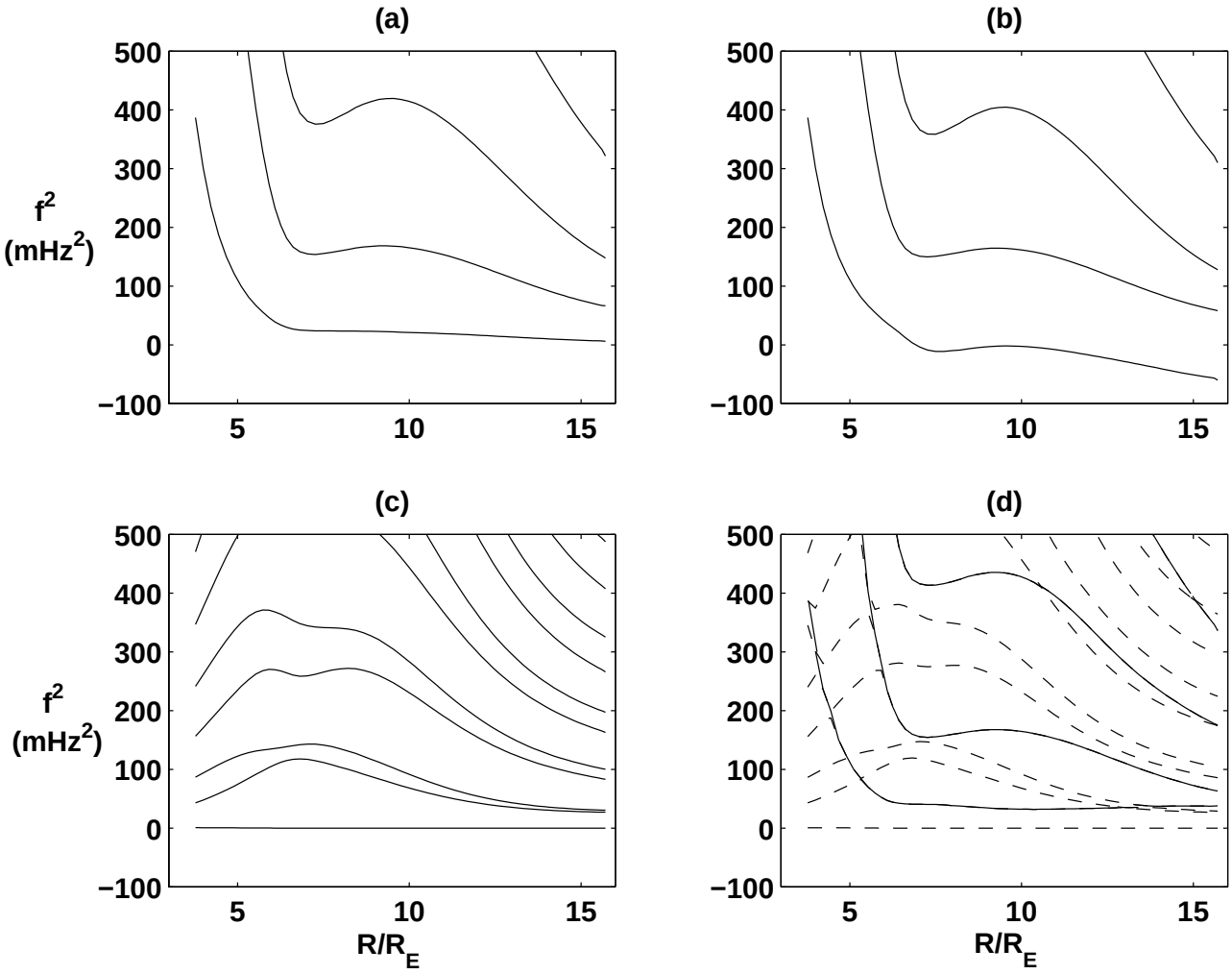

Figure 12. The square of frequency (in mHz) of field line resonance harmonics, f^2, versus the field line equatorial distance R (in R_E) for field lines with a constant α that corresponds to the local time 22:55:12 at the Earth for a disturbed time magnetosphere. (a) is for shear Alfvén waves in the cold plasma model limit, (b) is for shear Alfvén waves in the un-coupled warm plasma MHD model, (c) is for slow magnetosonic modes in the un-coupled warm plasma MHD model, and (d) is for shear Alfvén waves and slow modes in the coupled warm plasma MHD model.

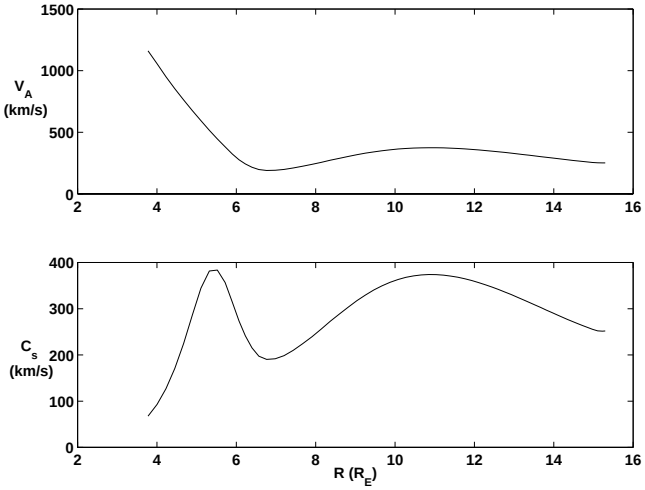

Figure 13. (a) Alfvén speed, $V_A = B/\rho^{1/2}$, and (b) slow magnetosonic speed, $C_s = (\Gamma_s P B^2/\rho(\Gamma_s P + B^2))^{1/2}$, (in km/s) versus the field line equatorial distance R (in R_E) for field lines with a constant α that corresponds to the local time 22:55:12 at the Earth for a disturbed time magnetosphere.

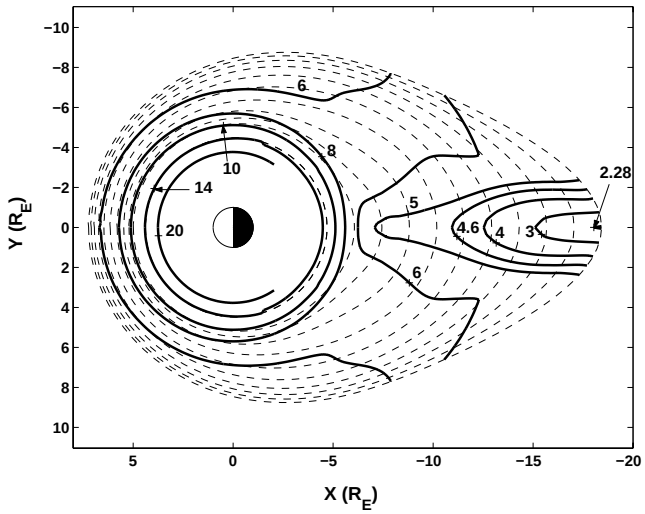

Figure 14. Contours of the fundamental harmonic shear Alfvén resonance frequency (in mHz) are plotted in the equatorial plane for a disturbed time magnetosphere. The dashed curves are the intersection of constant ψ surfaces with the equatorial plane.

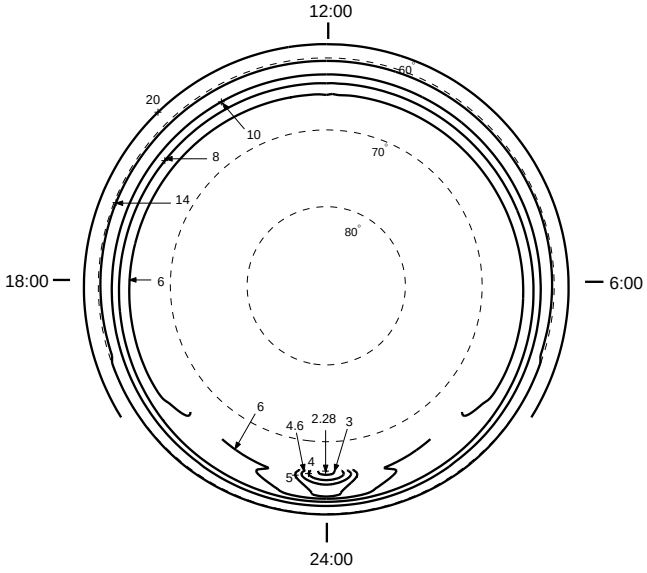

Figure 15. Contours of the fundamental harmonic shear Alfvén resonance frequency (in mHz) are plotted in the northern polar ionosphere for a disturbed time magnetosphere. The dashed circles are constant dipole latitude lines.

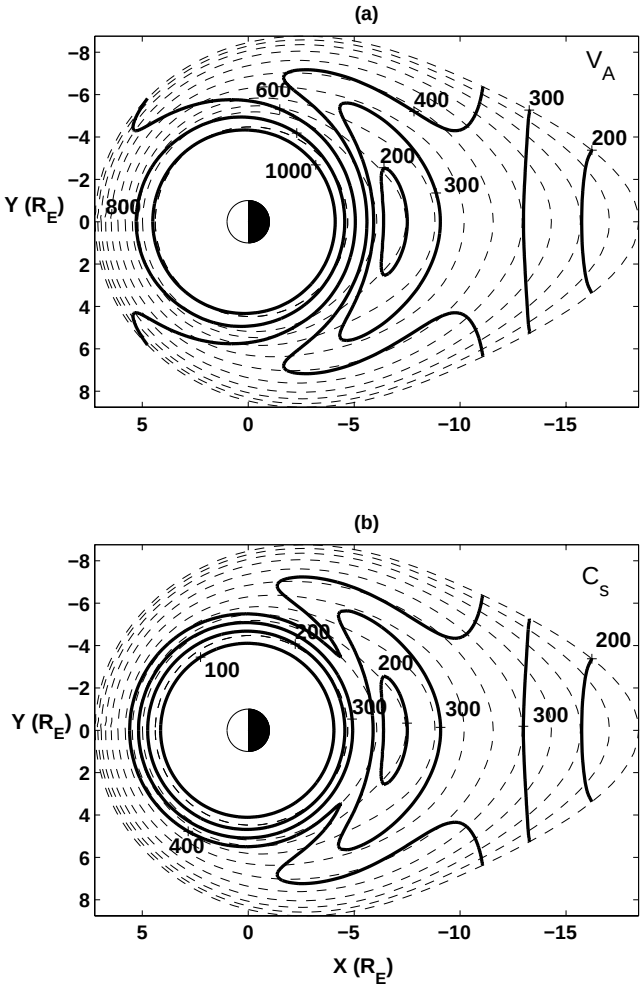

Figure 16. Contours of (a) Alfvén speed, $V_A = B/\rho^{1/2}$, and (b) slow magnetosonic speed, $C_s = (\Gamma_s P B^2/\rho(\Gamma_s P + B^2))^{1/2}$, (in km/s) in the equatorial plane for a disturbed time magnetosphere. The dashed curves are the intersection of constant ψ surfaces with the equatorial plane.

External Distribution

Plasma Research Laboratory, Australian National University, Australia
Professor I.R. Jones, Flinders University, Australia
Professor João Canalle, Instituto de Fisica DEQ/IF - UERJ, Brazil
Mr. Gerson O. Ludwig, Instituto Nacional de Pesquisas, Brazil
Dr. P.H. Sakanaka, Instituto Fisica, Brazil
The Librarian, Culham Laboratory, England
Library, R61, Rutherford Appleton Laboratory, England
Mrs. S.A. Hutchinson, JET Library, England
Professor M.N. Bussac, Ecole Polytechnique, France
Librarian, Max-Planck-Institut für Plasmaphysik, Germany
Jolan Moldvai, Reports Library, MTA KFKI-ATKI, Hungary
Dr. P. Kaw, Institute for Plasma Research, India
Ms. P.J. Pathak, Librarian, Insitute for Plasma Research, India
Ms. Clelia De Palo, Associazione EURATOM-ENEA, Italy
Dr. G. Grosso, Instituto di Fisica del Plasma, Italy
Librarian, Naka Fusion Research Establishment, JAERI, Japan
Library, Plasma Physics Laboratory, Kyoto University, Japan
Research Information Center, National Institute for Fusion Science, Japan
Dr. O. Mitarai, Kyushu Tokai University, Japan
Library, Academia Sinica, Institute of Plasma Physics, People's Republic of China
Shih-Tung Tsai, Institute of Physics, Chinese Academy of Sciences, People's Republic of China
Dr. S. Mirnov, TRINITI, Troitsk, Russian Federation, Russia
Dr. V.S. Strelkov, Kurchatov Institute, Russian Federation, Russia
Professor Peter Lukac, Katedra Fyziky Plazmy MFF UK, Mlynska dolina F-2, Komenskeho Univerzita, SK-842 15 Bratislava, Slovakia
Dr. G.S. Lee, Korea Basic Science Institute, South Korea
Mr. Dennis Bruggink, Fusion Library, University of Wisconsin, USA
Institute for Plasma Research, University of Maryland, USA
Librarian, Fusion Energy Division, Oak Ridge National Laboratory, USA
Librarian, Institute of Fusion Studies, University of Texas, USA
Librarian, Magnetic Fusion Program, Lawrence Livermore National Laboratory, USA
Library, General Atomics, USA
Plasma Physics Group, Fusion Energy Research Program, University of California at San Diego, USA
Plasma Physics Library, Columbia University, USA
Alkesh Punjabi, Center for Fusion Research and Training, Hampton University, USA
Dr. W.M. Stacey, Fusion Research Center, Georgia Institute of Technology, USA
Dr. John Willis, U.S. Department of Energy, Office of Fusion Energy Sciences, USA
Mr. Paul H. Wright, Indianapolis, Indiana, USA

The Princeton Plasma Physics Laboratory is operated
by Princeton University under contract
with the U.S. Department of Energy.

Information Services
Princeton Plasma Physics Laboratory
P.O. Box 451
Princeton, NJ 08543

Phone: 609-243-2750
Fax: 609-243-2751
e-mail: pppl_info@pppl.gov
Internet Address: http://www.pppl.gov